PARAMETRIC INVESTIGATION OF ORGANIC RANKINE CYCLE EVAPORATOR FOR LOW TEMPERATURE APPLICATIONS

U. Suhas* and G. Veershetty

Department of Mechanical Engineering, National Institute of Technology Karnataka, Mangalore, India.

ABSTRACT: The present work deals with the development of thermodynamic model of low temperature basic Organic Rankine Cycle (ORC) system and a chevron plate heat exchanger evaporator sub-model using Engineering Equation Solver (EES). Work output is evaluated using the ORC thermodynamic model, while the evaporator sub-model calculates the total surface area of the heat exchanger. Using these mathematical models, the effect of evaporation pressure, expander inlet temperature and pinch point temperature difference (PPTD) on the network output and evaporator cost are studied. In addition to this, the effect of plate spacing and plate width of chevron plate heat exchanger on pressure drop and evaporator cost are analyzed in detail. Finally, thermodynamic and geometric optimization is carried out using genetic algorithm to identify the optimum parameters at which the network output is maximized and pressure drop in the evaporator is minimized. Sensitivity analysis showed that optimum evaporator pressure existed at which network output is maximum. Thermodynamic optimization showed that work output was maximum (5.03 kW) at evaporator pressure of 5.77 bar. No improvement in the work output was seen with increase in PPTD and expander inlet temperature. Increase in plate width and plate spacing led to increase in evaporator cost and decrease in pressure drop.

Keywords: Evaporator; Genetic algorithm; Plate heat exchanger; Optimization; Sensitivity analysis; Thermodynamic model.

التحقيق البارمتري لمبخر دورة رانكين العضوية للتطبيقات ذات درجة الحرارة المنخفضة

ي . سوهاس*، ج . فيرشيتي

الملخص: يتناول العمل الحالي تطوير النموذج الديناميكي الحراري للنظام الأساسي لدورة رانكين العضوية (ORC) ذو درجة الحرارة المنخفضة والنموذج الفرعي لمبخر المبادل الحراري لألواح شيفرون باستخدام محلل المعادلات الهندسية. (EES) قمنا بتقييم ناتج العمل باستخدام النموذج الديناميكي الحراري ORC، بينما استخدمنا النموذج الفرعي للمبخر لاحتساب المساحة الكلية لمبادل الحرارة . وباستخدام هذه النماذج الرياضية، قمنا بدراسة تأثير ضغط التبخر ودرجة حرارة مدخل الموسع وفرق درجة حرارة نقطة القرص (PPTD) على صافي ناتج وتكلفة المبخر. بالإضافة إلى ذلك، حللنا تأثير تباعد اللوح وعرض لوح مبادل حراري شيفرون على انخفاض الضغط وتكلفة المبخر بالتفصيل. وأخيرًا، قمنا بإجراء التحسين الديناميكي الحراري والهندسي باستخدام الخوارزمية الجينية لتحديد المعاملات المثلى التي يتم عندها زيادة صافي الناتج وتقليل انخفاض الضغط في المبخر. و قد أظهر تحليل الحساسية أن الضغط الامثل للمبخر يكون عند وصول الحد الأقصى لصافي الناتج. كما أظهر التحسين الديناميكي الحراري أن أقصى إنتاج كان (5.03 كيلو واط) عند ضغط المبخر5.77 بار. هذا ولم يلحظ أي تحسن في الناتج مع زيادة وفرق درجة حرارة نقطة القرص ودرجة حرارة مدخل الموسع. كما أدت الزيادة في عرض اللوح وتباعد الألواح إلى زيادة في تكلفة المبخر ونقص في انخفاض الضغط.

الكلمات المفتاحية: المبخر؛ الخوارزمية الجينية؛ لوح مبادل الحرارة؛ التحسسينات؛ تحليل الحساسية؛ نموذج الديناميكا الحرارية؛ صافي الناتج.

*Corresponding author's e-mail: suhas.upa@gmail.com

DOI: 10.24200/tjer.vol16iss2pp130-141

NOMENCLATURE

A	Area of the heat exchanger, m^2
B	Plate spacing, m
B_o	Boiling number
D_h	Hydraulic diameter, m
DT_sup	Degree of superheat, °C
DP	Pressure drop, bar
f	Friction factor
G	Mass velocity, kg/m^2s
Ge_1,Ge_2,Ge_3,Ge_4	Non dimensional geometric parameter
h	Enthalpy, J/kg
h_{fg}	Enthalpy of vaporization, J/kg
k	Thermal conductivity, W/m K
L	Length of the plate, m
M_1	Mass flow rate of the working in kg/s
M_2	Mass flow rate of the heat transfer fluid in kg/s
N	No of segments in evaporation zone
Nu	Nusselt number
P	Pressure, bar
P_{co}	Corrugation pitch, mm
Pr	Prandtl number
q''	Average heat flux (W/m^2)
Q	Heat transfer rate, kW
Re	Reynolds number
t	Plate thickness, m
T	Temperature, °C
v	Specific volume, m^3/kg
w	Plate width, m
$\dot{W}$	work output, kW
x	Vapor quality
α	Convective heat transfer coefficient (W/m^2K)
β	Chevron angle (Degree)
ρ	Density (kg/m^3)
μ	Viscosity (kg/m s)
η	Efficiency
η_t	Isentropic efficiency of the expander
1,2,3,4	Thermodynamic states
in	input
cd	Condenser
ev	Evaporator
f	fluid phase
g	Vapor phase
hf	Hot fluid
p	Plate
pp	Pump
r	Refrigerant
sp	Single phase
th	thermal
tp	Two phase
w	Water side
wf	Working fluid
ORC	Organic Rankine cycle
PPTD	Pinch point temperature difference, °C
LMTD	Log mean temperature difference, °C

1. INTRODUCTION

Extraction of heat from low temperature sources has become inevitable along with other alternative sources of energy such as solar, wind etc. This is due to rapid urbanization and industrialization. Climate change and global warming has forced the policy makers in various countries to adopt green technologies (Arnaud *et al.* 2017). In recent years, a significant amount of research work has been done on Organic Rankine Cycle (ORC) technology. Low grade heat can be effectively utilized using ORC. Heat is absorbed by the organic fluid with low boiling point, in the evaporator. The high-pressure vapor is then passed through the expander which produces power (Usman *et al.* 2015). Man *et al.* (2013) analyzed a solar flat plate collector driven regenerative ORC and concluded that system performance improves at higher expander inlet temperature and lower condensation pressure. Wang *et al.* (2010) examined the performance of a solar operated ORC system by using evacuated tube and flat plate collectors as a source of heat for the ORC power block. They concluded that overall efficiencies of 4.2% and 3.2% were achieved with the evacuated solar collector and flat plate collector respectively. Pei *et al.* (2010) performed a numerical simulation of a low temperature solar thermal regenerative ORC system by using small concentration ratio compound parabolic collectors were used. They found that regeneration had a positive effect on the ORC efficiency. However, collector efficiency declined due to increase in the collector operating temperature. Francesco *et al.* (2015) simulated a 6 kWe solar power plant using TRNSYS software by assessing the system performance. They demonstrated that the efficiency throughout the year remained almost constant despite seasonal fluctuations. Some researchers have also studied ORC systems using other heat sources such as waste heat (Evangelos and Christos, 2018; Filiz *et al.* 2015; Imran *et al.* 2014; Jian *et al.* 2015; Jiangfeng *et al.* 2013; and Seyedali *et al.* 2017), biomass combustion (Riffat 2012; Roshaan *et al.* 2017) and geothermal (Hossein *et al.* 2017; Xinghua *et al.* 2017).

ORC performance mainly depends on heat exchangers, expander and choice of working fluid. Moreover, the effect of operating conditions is significant. In the recent past, researchers have focused on these aspects. Dai *et al.* (2009) carried out parametric optimization of ORC for low grade waste heat recovery. Their studies showed that, the presence of recuperator within the ORC power block did not contribute to the betterment of ORC efficiency, under the given waste heat conditions. Onder Kaska (2014) analyzed a waste heat recovery ORC in steel industry. In his/her study, exergy losses in each ORC component were assessed by using actual plant data. Maximum rate of irreversibility was observed in the evaporator followed by expander, condenser and pump. Higher evaporator pressures yielded greater thermal and exergy efficiencies. Sahar Safarian and Fereshteh Aramoun (2015) conducted a detailed energy and exergy analysis of 4 different configurations of ORC; Basic, regenerative, turbine bled and both Regenerative and turbine bleeding. They concluded that regenerative ORC with turbine bleeding outperformed the rest in terms of energy and exergy efficiency. Significant work has been carried out on parametric optimization of various ORC configurations and applications, using different working fluids. Imran *et al.* (2015) developed a thermal and hydraulic design model of a plate heat exchanger, for a low temperature ORC system. Using the model, they optimized its geometrical parameters with Genetic Algorithm. Evaporator cost and pressure drop were chosen as objective functions. Plate length, width and spacing were chosen as decision variables. They concluded that the plate length had a significant effect on the evaporator pressure drop and cost.

Thermodynamic and cost assessment of plate heat exchanger for low temperature ORC applications is very limited in the open literature. This work consists of three parts. In the first part of this study, a parametric investigation is carried out to study the effect of thermodynamic parameters on the cost and performance of the plate heat exchanger. The effect of geometrical parameters of the heat exchanger on cost and pressure drop are analyzed in the second part. Finally, thermodynamic and geometric optimization is carried out for maximizing work output and minimizing pressure drop respectively using genetic algorithm. The main objectives of the study are:
a) to develop a thermodynamic model to evaluate the network output of the system; b) to develop a plate heat exchanger evaporator sub-model to estimate the surface area of the evaporator and hence, the cost of the heat exchanger; c) to examine the effect of thermodynamic and geometrical parameters of the plate heat exchanger on its cost and work output of the ORC system; d) to optimize thermodynamic parameters to maximize network output of ORC system using genetic algorithm; and e) to minimize pressure drop by optimizing the geometrical parameters of the evaporator, using genetic algorithm.

2. SYSTEM DESCRIPTION

In this study, a low-temperature organic Rankine cycle power generation system is assessed. R245fa is used as the working fluid because of its lower operating pressure compared to other ORC working fluids and is preferred for small-scale power generation. Thermophysical properties and other important characteristics of R245fa are listed in Table 1. The ORC power block consists of a working fluid pump to pump the fluid to the desired pressure as shown in Fig. 1.

This pressurized fluid is then passed on to the evaporator where heat addition takes place. The

pressurized vapor passes through the expander, where the actual expansion of the working fluid takes place and the pressure drops. Finally, the vapor condenses in the condenser to complete the cycle.

3. THERMODYNAMIC ANALYSIS

The governing equations used in the model are explained in section 3.1 and 3.2. Plate type heat exchangers are used as evaporators in small scale ORC power plants, because they are compact and have better heat transfers coefficients when compared to shell and tube heat exchangers. The plate heat exchanger is divided into three zones *i.e.* preheating zone, 2 phase zone and superheating zone as shown in Fig. 2. Under the considered operating conditions, each section is designed separately using Logarithmic Mean Temperature Difference method.

The following assumptions were made to simplify the analysis.

a) The system is in a steady state.
b) R245fa is in a saturated condition at the condenser outlet.
c) Isentropic efficiency of pump and expander are constant at 70%.
d) The fouling effects of the heat exchanger are negligible.

The program was written in function format using Engineering Equation Solver (EES). The design process is iterative and the iterations were carried out until pressure drop on the cold side of the evaporator converged. The evaporator was redesigned for each iteration and its cost was evaluated based on the surface area of the heat exchanger.

Table 1. Thermophysical properties of R245fa.

Sl	Property	Value	Unit
1	Molecular mass	134.05	kg/K-mol
2	Critical temperature	154.01	°C
3	Critical pressure	3.64	MPa
4	Boiling point	15.14	°C
5	Ozone depletion potential	0	-
6	Global warming potential	950	/100 year

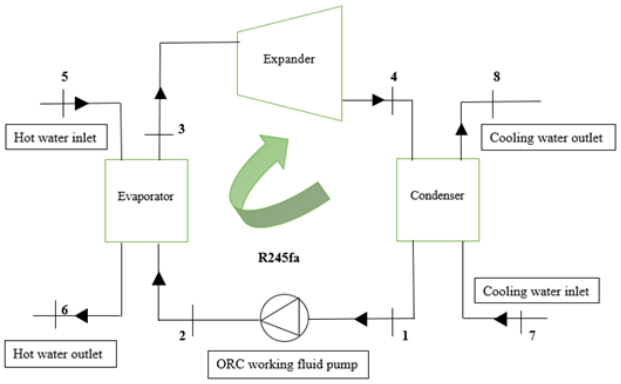

Figure 1. Schematic demonstration of a low temperature organic Rankine cycle system.

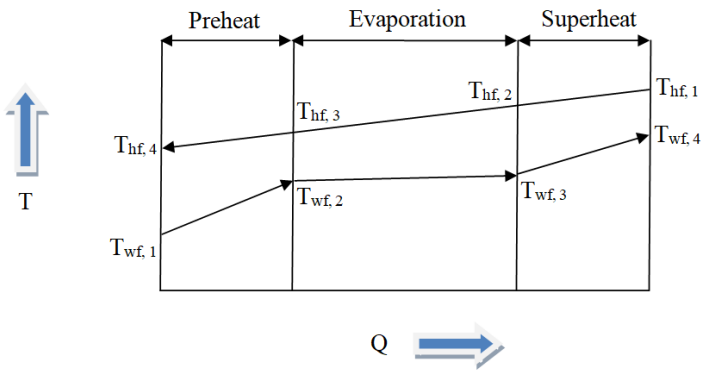

Figure 2. Temperature profile in the evaporator.

3.1 Thermodynamic Model of ORC System

The main aim of the model was to estimate the surface area of the chevron plate heat exchanger for the given inputs as mentioned in Table 2. Sensitivity analysis was carried out using this model to analyze the effect of thermodynamic and geometric parameters on the work output and the cost of the system.

Heat balance equations used in the ORC model are as follows:

Preheat zone

$$M_2 \times (h_{hf,3} - h_{hf,4}) = M_1 \times (h_{wf,2} - h_{wf,1}) \quad (1)$$

Superheating zone

$$M_2 \times (h_{hf,1} - h_{hf,2}) = M_1 \times (h_{wf,4} - h_{wf,3}) \quad (2)$$

Based on inlet and exit

$$M_2 \times (h_{hf,1} - h_{hf,4}) = M_1 \times (h_{wf,4} - h_{wf,1}) \quad (3)$$

Pinch point is the location in a heat exchanger where the difference in temperature of hot and cold fluids is minimum. This is represented as,

$$PPTD = T_{hf,3} - T_{wf,2} \quad (4)$$

Calculation of network output

Pump work is given by,

$$\dot{W}_{PP} = M_1 x\, v_1 \times \frac{(p_2 - p_1)}{\eta_{pp}} \quad (5)$$

The heat addition in the evaporator,

$$\dot{Q} = M_1 \times (h_3 - h_2) \quad (6)$$

Isentropic efficiency of the expander is calculated as the ratio of actual work done by the expander to that of the isentropic work done by the expander.

$$\eta_t = \frac{h_3 - h_4}{h_3 - h_{4s}} \quad (7)$$

Actual work done by the expander,

$$\dot{W}_t = M_1 \times (h_3 - h_4) \quad (8)$$

For a given isentropic efficiency of the expander, the actual work done by the expander can be calculated as,

$$\dot{W}_t = M_1 \times (h_3 - h_{4s}) \times \eta_t \quad (9)$$

Network output is evaluated as,

$$\dot{W}_{net} = \dot{W}_t - \dot{W}_{pp} \quad (10)$$

Thermal efficiency is evaluated as,

$$\eta_{th} = \frac{\dot{W}_{net}}{\dot{Q}} \quad (11)$$

3.2 Evaporator Sub-Model

3.2.1 Single phase

The heat transfer is calculated as,

$$Q_{sp} = U_{sp} \times A_{sp} \times LMTD_{sp} \quad (12)$$

Log mean temperature difference,

$$LMTD_{sp} = \frac{\Delta T_{max} - \Delta T_{min}}{\ln\left(\frac{\Delta T_{max}}{\Delta T_{min}}\right)} \quad (13)$$

The overall heat transfer coefficient of single phase (Imran *et al*. 2014),

Table 2. Inputs to the model.

Sl No	Symbol	Parameter	Value	Unit
1	D_h	Hydraulic diameter	0.0035	m
2	β	Chevron angle	45	Degree
3	P_{co}	Corrugation pitch	0.007	m
4	k_p	Thermal conductivity of the plate	13.5	W/m-K
5	N	Number of segments in evaporation zone	20	-
6	t_p	Thickness of the plate	0.0005	m
7	η_p	Isentropic efficiency of pump	70	%
8	η_t	Isentropic efficiency of expander	70	%
9	M_2	Mass flow rate	0.7	kg/s

$$\frac{1}{U_{sp}} = \frac{1}{\alpha_w} + \frac{t_p}{k_p} + \frac{1}{\alpha_{r,sp}} \quad (14)$$

The convective heat transfer coefficient for R245fa in plate heat exchanger is calculated as (Imran *et al*. 2015),

$$\alpha_{r,sp} = 0.2092 \times \left(\frac{k_f}{D_h}\right) \times Re^{0.78} \times Pr^{0.33} \times \left(\frac{\mu_m}{\mu_{wall}}\right)^{0.14} \quad (15)$$

3.2.2 Two phases

In this region, the correlations used in single phase, based on constant fluid properties cannot be used. The fluid properties tend to vary as the quality of the fluid changes. Therefore, a modified LMTD method is employed.

The evaporation region is discretised into 'N' smaller sections so that there are incremental changes in fluid properties at each section. Therefore, constant fluid properties are assumed in each section. In this analysis, the value of N was restricted to 20 as the processing time of the model increased when the value of 'N' was increased and negligible change in the evaporator area was observed.

The heat transfer rate for i^{th} section is evaluated as

$$Q_i = U_i \times A_i \times LMTD_i \quad (16)$$

Log mean temperature difference,

$$LMTD_i = \frac{\Delta T_{max,i} - \Delta T_{min,i}}{\ln\left(\frac{\Delta T_{max,i}}{\Delta T_{min,i}}\right)} \quad (17)$$

The two-phase overall heat transfer coefficient (Imran *et al*. 2014),

$$\frac{1}{U_{tp,i}} = \frac{1}{\alpha_{w,i}} + \frac{t_p}{k_p} + \frac{1}{\alpha_{r,sp,i}} \quad (18)$$

The Nusselt No. correlation for R245fa evaporation in plate heat exchanger (Han *et al*. 2003)

$$Nu_{tp} = Ge_1 \times Re_{eq}^{Ge_2} \times Bo_{eq}^{0.3} \times Pr^{0.4} \quad (19)$$

where,

$$Ge_1 = 2.81 \times \left(\frac{P_{co}}{D_h}\right)^{-0.041} \left(\frac{\pi}{2} - \beta\right)^{-2.83} \quad (20)$$

$$Ge_2 = 0.746 \times \left(\frac{P_{co}}{D_h}\right)^{-0.082} \times \left(\frac{\pi}{2} - \beta\right)^{0.61} \quad (21)$$

The equivalent Reynolds number and boiling number are given by,

$$Re_{eq} = \frac{Ge_{eq} \times D_h}{\mu_f} \quad (22)$$

$$Bo_{eq} = \frac{q''}{Ge_{eq} \times h_{fg}} \quad (23)$$

$$Ge_{eq} = G\left[(1 - x) + x\left(\frac{\rho_f}{\rho_g}\right)^{0.5}\right] \quad (24)$$

where, *G* denotes the mass velocity and D_h represents the hydraulic diameter of the flow channel.

$$D_h = \frac{(4 \times A)}{P} = \frac{(4 \times W \times b)}{2 \times (W + b)} \quad (25)$$

where, *w* is the plate width and b is the plate spacing (Jiangfeng *et al*. 2013).

Frictional pressure drop is calculated as (Imran *et al*. 2014),

$$\Delta P = \frac{4 \times f \times L \times G^2}{2 \times \rho \times D_h} \quad (26)$$

A single phase frictional pressure drop factor is given by (Imran *et al*. 2015),

$$f = \frac{0.572}{Re^{0.217}} \quad (27)$$

Two phase frictional factor is expressed as (Han *et al*. 2003),

$$f = Ge_3 \times Re_{eq}^{Ge_4} \quad (28)$$

$$Ge_3 = 64710 \times \left(\frac{P_{co}}{D_h}\right)^{-5.27} \times \left(\frac{\pi}{2} - \beta\right)^{-3.03} \quad (29)$$

$$Ge_4 = -1.314 \times \left(\frac{P_{co}}{D_h}\right)^{-0.62} \times \left(\frac{\pi}{2} - \beta\right)^{-0.47} \quad (30)$$

Cost of evaporator

Evaporator cost is linearly related to evaporator heat transfer area (Imran *et al*. 2015) and is given by,

$$\text{Cost of the evaporator (US\$)} = 310 + (160 \times A), \quad (31)$$

Where, *A* is the heat transfer area in m^2

4. RESULTS AND DISCUSSION

Parametric investigation is carried out to examine the effect of each thermodynamic parameter on the performance of the ORC system. The effect of heat exchanger geometry on the cost and pressure drop is also analyzed in detail. In this study, the parameter to be investigated is varied whereas others are kept constant. The effect of thermodynamic parameters on the ORC system performance is discussed in Section 4.1. Section 4.2 highlights the effect of geometrical parameters of the heat exchanger on the evaporator cost and pressure drop.

4.1 Effect of Thermodynamic Parameters on System Performance

4.1.1 Evaporator pressure

The heat source temperature and the condensation temperature were set at 100 °C and 40 °C respectively. Evaporator pinch point temperature and degree of superheat were kept constant at 5 °C. Evaporator pressure was varied from 4 to 10 bar. Figure 3 shows the effect of evaporator pressure on the network output and thermal efficiency when R245fa is used as the working fluid. It can be observed that the work output increases initially and then declines. Hence, for a given working fluid, there exists an optimum evaporator pressure at which, work output is maximum. Mass flow rate of the working fluid decreases with an increase in evaporator pressure as shown in Fig. 4. The initial increase in the work output is due to the higher enthalpy difference across the expander. But, when the pressure is increased beyond 6 bar, the effect of reduced mass flow rate outweighs the increase in enthalpy difference across the expander. This results in reduction of network output at higher evaporator pressure. In case of thermal efficiency, at higher pressures, in addition to the network output being higher, the heat input to the system decreases. Latent heat of vaporization decreases as the evaporation pressure increases. Therefore, the thermal efficiency increases with an increase in evaporator pressure. Figure 5 shows the effect of evaporator pressure on the evaporator area. The surface area decreases with an increase in evaporator pressure. Evaporation temperature increases as a result of increasing evaporator pressure. As the pinch point temperature difference (PPTD) remains constant, the exit temperature of the heat transfer fluid increases correspondingly. As a consequence of this, heat transfer rate decreases in the evaporator. Hence, reduction in the evaporator surface area is observed with an increase in evaporator pressure. Figure 6 depicts the variation of the evaporator with evaporator pressure cost. Since, the evaporator area decreases with the increase in evaporator pressure, the cost also decreases. However, in practical applications, the evaporator surface area cannot be varied. Therefore, this theoretical study only helps the designer to identify the operating condition of ORC where the evaporator area (and hence, the cost) is minimum.

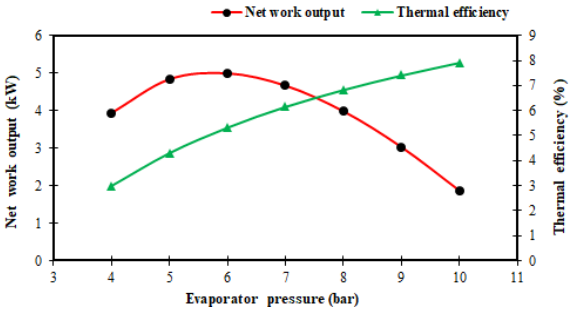

Figure 3. Effect of evaporator pressure on network output and thermal efficiency.

4.1.2 Pinch point temperature difference

The heat source temperature and the condensation temperature were set at 100 °C and 40 °C respectively. Evaporator pressure was fixed at 8 bar. Superheat degree was maintained constant at 5 °C. The pinch point temperature difference was varied from 2 °C to 14 °C. When the pinch point temperature is increased while maintaining all other parameters constant, hot fluid exit temperature, $T_{hf,\ 3}$, increases. However, since, expander inlet and exit conditions remain constant, by energy balance, mass flow rate of the working fluid decreases as shown in Fig. 8. This also explains the reduction in the network output as indicated in Fig. 7. Moreover, change in PPTD does not have any impact on the thermal efficiency. As PPTD is varied, both network output and heat added to the cycle decreases proportionately. Therefore, the ratio of work output to heat added to the cycle remains unaffected.

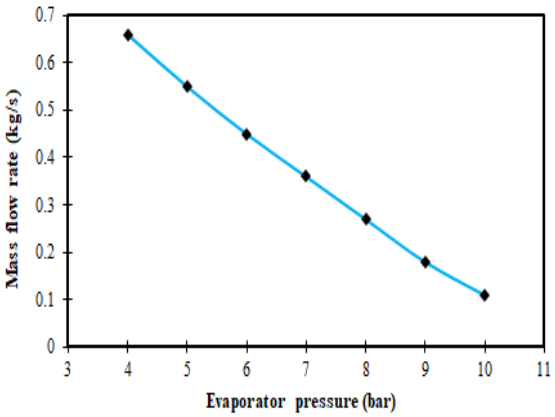

Figure 4. Effect of evaporator pressure on mass flow rate.

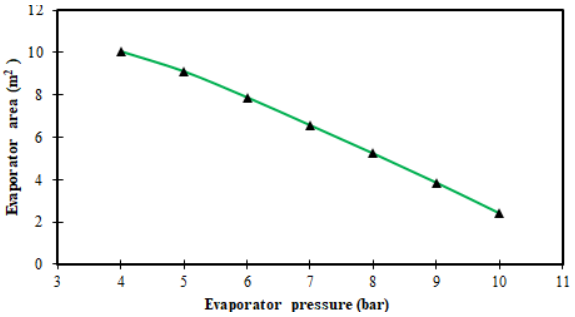

Figure 5. Effect of evaporator pressure on evaporator area.

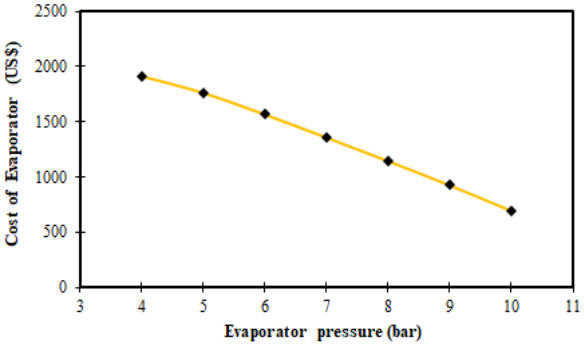

Figure 6. Effect of evaporator pressure on evaporator cost.

Figure. 9 shows the effect of PPTD on the evaporator area. In addition to the reduction in mass flow rate, log mean temperature difference also increases. As a result of this, the heat exchanger area decreases with an increase in PPTD. The cost of the evaporator decreases because of the reduction in the evaporator surface area as indicated in Fig. 10.

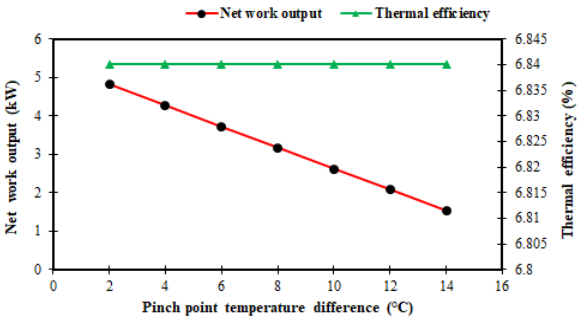

Figure 7. Effect of pinch point temperature difference on network output and thermal efficiency.

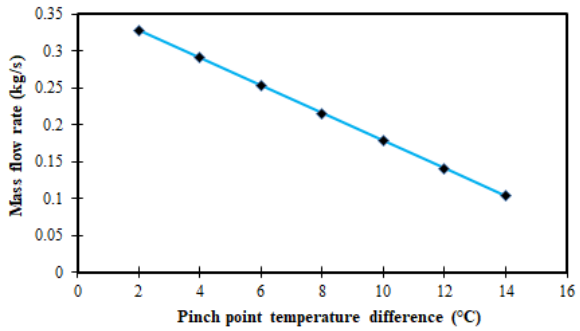

Figure 8. Effect of pinch point temperature difference on mass flow rate.

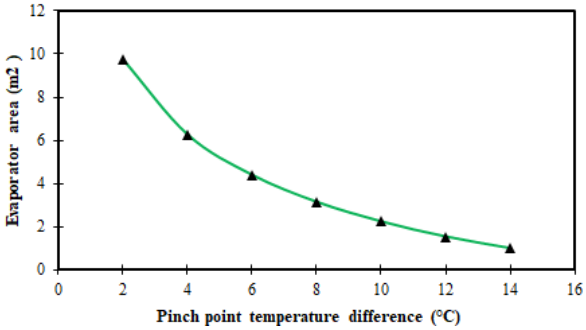

Figure 9. Effect of pinch point temperature difference on evaporator area.

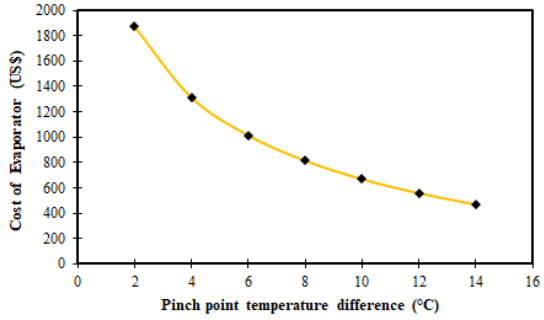

Figure 10. Effect of pinch point temperature difference on evaporator cost.

4.1.3 Expander inlet temperature

The heat source temperature and the condensation temperature were set at 100 °C and 40 °C respectively. The pinch point temperature difference was set at 5 °C. The evaporator pressure was kept constant at 6.96 bar (corresponding to saturation temperature of 75 °C). The degree of superheat was then increased up to 20 °C. With the increase in expander inlet temperature, the enthalpy difference across the expander increases. Hence, according to energy balance, the mass flow rate of the working fluid decreases as depicted in Fig. 12. Figure 11 indicates the reduction in net power output and thermal efficiency. This is because, the marginal gain in enthalpy drop across the expander is lesser than the rate of decrease of mass flow rate.

Figure 13 shows the variation of evaporator surface area with expander inlet temperature. With an increase in expander inlet temperature, the area reduces initially, then increases again. Due to the constraint of PPTD, the mass flow rate decreases by energy balance. Hence, there is a significant reduction in heat transfer rate in the evaporation section. This effect is predominant at lower expander inlet temperatures. As the inlet temperature is increased further, the log mean

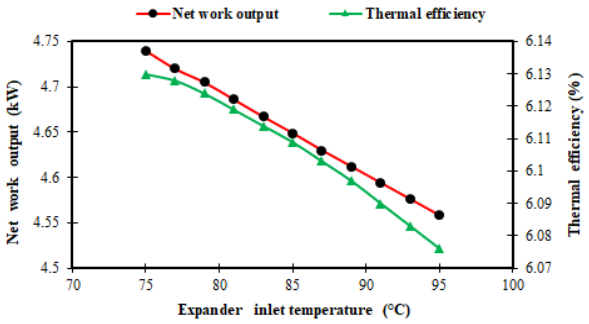

Figure 11. Effect of expander inlet temperature on network output and thermal efficiency.

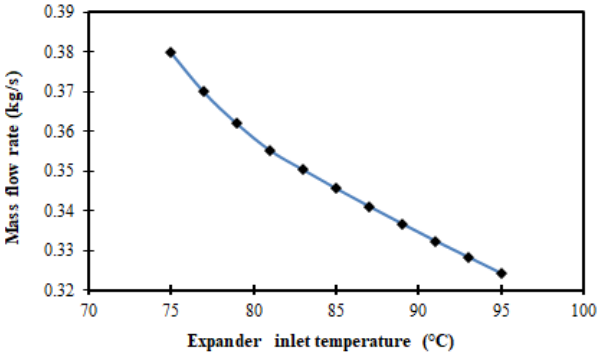

Figure 12. Effect of expander inlet temperature on mass flow rate.

temperature difference in the superheat zone also decreases. This results in increase in the superheated zone area. This phenomenon explains the increase in the evaporator area at higher expander inlet temperatures. The evaporator cost also exhibits the same trend as that of the evaporator area as shown in Fig. 14. It can be seen that, for dry fluids such as R245fa, increasing expander inlet temperature by more than 5 °C, will not yield any positive results as the surface area requirement of the evaporator and cost increases. Moreover, work output also reduces due to lower mass flow rates.

4.2 Effect of Geometrical Parameters on Pressure Drop and Evaporator Cost

Plate spacing was kept constant at 0.003 m and the width of the plate was varied from 0.005 m to 0.009 m. Hydraulic diameter was calculated based on Eq. 24.

Figure 15 shows the effect of plate width on the cost of the evaporator and frictional pressure drop. As the width of the plate increases, the area increases slightly. This results in marginal increase in the evaporator cost. Increase in plate width also causes Reynolds number to increase. The frictional pressure drop is related to Reynolds number as shown in Eq 15. Therefore, total pressure drop in the plate heat exchanger reduces.

The variation of evaporator cost and frictional pressure drop with plate spacing is presented in Fig. 16. In this case, the plate width was fixed at 0.5 m and plate spacing was varied from 0.002 m to 0.005 m. The increase in plate spacing creates more space for indirect contact between the heat source and the working fluid. This leads to reduced heat transfer. To maintain constant heat transfer, additional plates have to be added, which leads to increase in the evaporator area, therefore the evaporator cost increases. When plate spacing is increased, the hydraulic diameter and Reynolds number increases. This directly impacts the frictional pressure drop. Frictional pressure drop reduces with increase in plate spacing.

4.3 Genetic Algorithm Optimization

As per the preceding analysis, parametric optimization is carried out using genetic algorithm (GA). The purpose of this study is: a) to maximize the work output by optimizing evaporator pressure, expander inlet temperature and pinch point temperature difference; and b) to minimize the pressure drop by optimizing the plate spacing and plate width in Chevron plate heat exchanger.

Genetic algorithm begins from a population of possible solutions. These are called *individuals*. This prevents the convergence of the algorithm to sub-optimal solutions. The algorithm moves towards the optimal one by applying the Darwinian principle of '*survival of the fittest'*. Fitness function is the criteria for selecting the individuals. The initial population is generated randomly. A new population is created by applying crossover and mutation operators to the selected individuals (parents). This technique differs from conventional optimization techniques as it involves search from a group of solutions. This

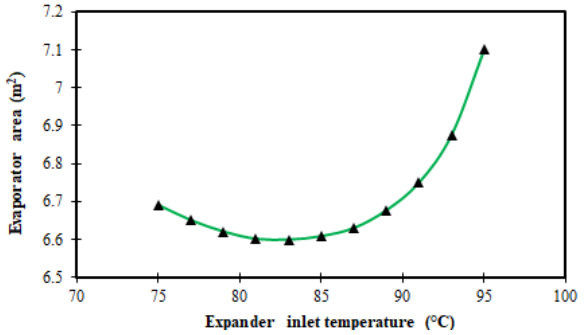

Figure 13. Effect of expander inlet temperature on evaporator area.

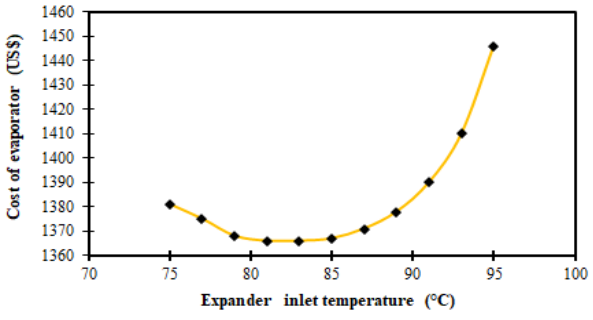

Figure 14. Effect of expander inlet temperature on evaporator cost.

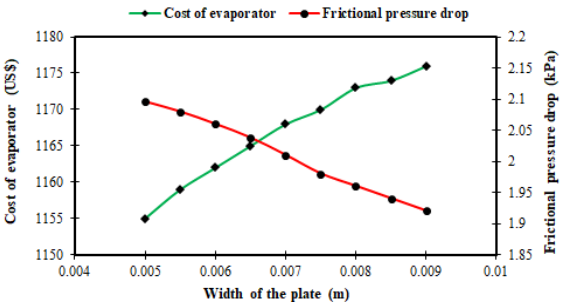

Figure 15. Effect of plate width on evaporator cost and frictional pressure drop.

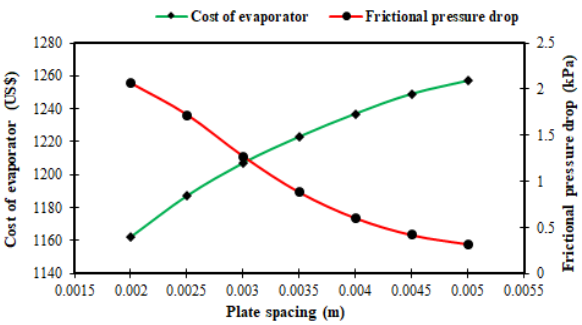

Figure 16. Effect of plate spacing on evaporator cost and frictional pressure drop.

prevents convergence to suboptimal solutions. The procedure is explained in the form a flowchart as shown in fig. 17.

4.3.1 Maximize network output

The objective function for the basic ORC cycle is given by,

Maximize ($\dot{W}_{net}$),
Subjected to constraints,
4 bar $\leq P_{ev} \leq$ 10 bar ;
5 $\leq$ superheat $\leq$ 20 ;
5 $\leq$ $PPTD_{ev} \leq$ 20 ;
$T_{hf,1}$ = 100 °C & T_{cd} = 40 °C

Input data for parametric optimization is presented in Table 3 and Table 4. Maximum evaporator pressure was fixed at 10 bar as this is the limiting pressure for scroll expanders. Heat source temperature and condensation temperature were kept constant at 100 °C and 40 °C respectively. Network output was chosen as the objective function. Fig. 3 showed that there exists an optimum evaporator pressure for which the work output is maximum. The optimization results are tabulated in Table 5 and Table 6. Maximum power output of 5.03 kW_e is attained at evaporator pressure of 5.77 bar. The increase in degree of superheat and pinch point temperature difference affects the network output of the system negatively, as seen from the results.

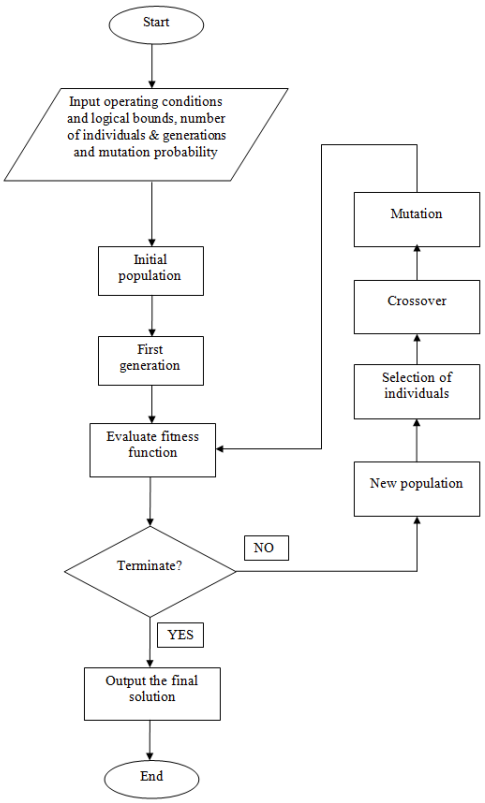

Figure 17. Simplified flowchart of genetic algorithm.

Table 3. Data of thermodynamic optimization for Maximizeing work output.

Working fluid	R245fa
Population size	64
Stop generation	128
Mutation probability	0.18
Range of evaporator pressure (bar)	4-10
Range of degree of superheat (ºC)	5-20
Range of Pinch point temperature difference (˚C)	5-20
Heat source temperature (˚C)	100
Condensation temperature (˚C)	40

Table 4. Data of geometric optimization for minimizing pressure drop.

Working fluid	R245fa
Population size	64
Stop generation	128
Mutation probability	0.175
Degree of superheat (˚C)	5
Evaporator pressure (bar)	5.77
Pinch point temperature difference	5.0
Range for plate width (m)	0.1-0.5
Range for plate spacing (m)	0.002 to 0.007

Table 5. Thermodynamic optimization results for maximum network output.

Parameter	Value	Unit
P	5.77	bar
DT_sup	5	˚C
PPTD	5.0	˚C
W_{net}	5.03	kW_e

Table 6. Geometric optimization results for minimum pressure drop.

Parameter	Value	Unit
Plate spacing	0.007	m
Plate width	0.5	m
Pressure drop	0.03076	kPa

4.3.2 Minimize pressure drop

The objective function is given by,

Minimize (DP),

Subjected to constraints,
$0.1 \leq w \leq 0.5$;
$0.002 \leq b \leq 0.007$
$P_{ev} = 5.77$ bar; DT_sup = 5 °C; $PPTD_{ev} = 5$ °C
(Optimized performance parameters for maximum network output)

In case of geometric optimization, only plate width and plate spacing were considered. The evaporator pressure was set at 5.77 bar (optimized condition), degree of superheat and pinch point temperature difference was fixed at 5 °C. The optimum value of plate width and plate spacing was evaluated so that pressure drop was minimum. The optimization results showed that plate width and plate spacing were at their upper limit set before the start of the optimization process. However, the increase in plate spacing and plate width results in increase in the evaporator area and the cost as indicated in Table 7. Therefore, a trade-off has to be made by the designer between cost and pressure drop requirements.

5. CONCLUSION

This study dealt with the effects of thermodynamic and geometric parameters on the performance and cost of the ORC system. Parametric optimization was carried out using Genetic algorithm. R245fa was used as the working fluid. The main conclusions are as follows:

1. Evaporator area decreases with increase in evaporator pressure resulting in the reduction of evaporator cost. Optimum evaporator pressure was found to be at 5.77 bar which resulted in maximum network output of 5.03 kW.
2. Network output decreased with increase in expander inlet temperature. Higher inlet temperature *ie*. degree of superheat greater than 5°C led to increase in evaporator cost.
3. Increase in Pinch point temperature difference resulted in decrease of network output and evaporator cost (because of smaller surface area).
4. Increase in plate width and plate spacing led to increase in evaporator cost and reduction in pressure drop.
5. A tradeoff has to be made between pressure drop and heat exchanger cost depending on the application.

Table 7. Variation of heat exchanger area with plate spacing and plate width.

Parameter	Value		Unit
Plate spacing	0.002	0.007	m
Plate width	0.1	0.5	m
Evaporator area	8.32	10	m^2

CONFLICT OF INTEREST

The authors declare no conflicts of interest.

FUNDING

National Institute of Technology, Karnataka Surathkal, India.

ACKNOWLEDGMENT

This project needed intensive literature review and latest research data which was provided by the National Institute of Technology, Karnataka Surathkal, India.

REFERENCES

Arnaud L, Nicolas T, Philippe H, Rémi R, and Stéphane C (2017), Organic Rankine cycle design and performance comparison based on experimental database, *Applied Energy*, 204: 1172-1187.

Dai Y, Jiangfeng W, Lin G (2009), Parametric optimization and comparative study of organic Rankine cycle (ORC) for low grade waste heat recovery, *Energy Conversion and Management*, 50: 576-582.

Evangelos B, Christos T (2018), Investigation of a hybrid ORC driven by waste heat and solar energy, *Energy Conversion and Management*,156: 427-439

Filiz T.O. N, Rıdvan S, Atakan T (2015), Thermodynamic analysis of an Organic Rankine Cycle (ORC) based on industrial data, *Applied Thermal Engineering*, 91: 43-52.

Francesco C, Massimo D d'Accadia, Maria V, Marco S (2015), Design and simulation of a prototype of a small-scale solar CHP system based on evacuated flat-plate solar collectors and Organic Rankine Cycle, *Energy Conversion and Management*, 90: 347–363.

Han Dong-Hyouck, Lee Kyu-Jung, Kim Yoon-Ho, (2003), Experiments on the characteristics of evaporation of R410A in brazed plate heat exchangers with different geometric configurations, *Applied Thermal Engineering*, 23: 1209-1225

Hossein N, Arash N, Farshad J.F. (2017), Conventional and advanced exergy analyses of a geothermal driven dual fluid organic Rankine cycle (ORC), *Applied Thermal Engineering*, 122: 59-70.

Imran M, Byung S.P. Hyouck J.K. Dong H.L, Muhammad U (2014), Thermo-economic optimization of regenerative organic Rankine cycle for waste heat recovery applications, *Energy Conversion and Management*, 87: 107–118.

Imran M, Muhammad U, Byung-Sik Park, Hyouck-Ju Kim, Dong-Hyun L (2015), Multi-objective optimization of evaporator of organic Rankine cycle (ORC) for low temperature geothermal heat source, *Applied Thermal Engineering*, 80: 1-9.

Jian S, Yin S, Chun-wei Gu (2015), Thermodynamic analysis and performance optimization of an Organic Rankine Cycle (ORC) waste heat recovery system for marine diesel engines, *Energy*, 82: 976-985.

Jiangfeng W, Zhequan Y, Man W, Shaolin M, Yiping D (2013), Thermodynamic analysis and optimization of an (organic Rankine cycle) ORC using low grade heat source, *Energy*, 49: 356-365.

Man W, Jiangfeng W, Yuzhu Z, Pan Z, Yiping D (2013), Thermodynamic analysis and optimization of a solar-driven regenerative organic Rankine cycle (ORC) based on flat-plate solar collectors, *Applied Thermal Engineering*, 50: 816-825.

Onder K (2014), Energy and exergy analysis of an organic Rankine for power generation from waste heat recovery in steel industry, *Energy Conversion and Management*, 77: 108-117.

Pei G, Li J, Ji J (2010), Analysis of low temperature solar thermal electric generation using regenerative Organic Rankine Cycle, *Applied Thermal Engineering*, 30: 998-1004.

Riffat (2012), Experimental investigation of a biomass-fired ORC-based micro-CHP for domestic applications, *Fuel*, 96: 374-382.

Roshaan M, Faraz A, Man-Hoe Kim (2017), Thermodynamic analysis of organic Rankine cycle used for flue gases from biogas combustion, *Energy Conversion and Management*, 153: 627-640.

Sahar S, Fereshteh A (2015), Energy and exergy assessments of modified OrganicRankine Cycles (ORCs), *Energy reports*, 1: 1-7.

Seyedali S, Saeed J, Krishna K (2017), Exergy-based optimization of an organic Rankine cycle (ORC) for waste heat recovery from an internal combustion engine (ICE), *Applied Thermal Engineering*, 126: 447-457.

Usman M, Muhammad I, Dong H.L, Byung S.P (2015), Design and experimental investigation of a 1 kW organic Rankine cycle system using R245fa as working fluid for low-grade waste heat recovery from steam, *Energy Conversion and Management*,103:1089-1100.

Wang X.D, Zhao L, Wang J.L. Zhang W.Z, Zhao X.Z, Wu W (2010), Performance evaluation of a low-temperature solar Rankine cycle system utilizing R245fa, *Solar Energy*, 84: 353-364.

Xinghua L, Yufeng Z, Jiang S (2017), System performance optimization of ORC-based geo-plant with R245fa under different geothermal water inlet temperatures, *Geothermics*, 66: 134-142.

Yiping D, Jiangfeng W, Lin G (2009), Parametric optimization and comparative study of organic Rankine cycle (ORC) for low grade waste heat recovery. *Energy Conversion and Management*, 50: 576-582.